Journal of Catalysis 272 (2010) 121–130

Contents lists available at ScienceDirect

Journal of Catalysis

journal homepage: www.elsevier.com/locate/jcat

Influence of the calcination temperature on the nano-structural properties, surface basicity, and catalytic behavior of alumina-supported lanthana samples

Zouhair Boukha [a], Loubna Fitian [a], Miguel López-Haro [a,b], Manuel Mora [c], José Rafael Ruiz [c], César Jiménez-Sanchidrián [c], Ginesa Blanco [a], José J. Calvino [a], Gustavo A. Cifredo [a], Susana Trasobares [a,b], Serafín Bernal [a,*]

[a] Departamento de Cencia de los Materiales e Ingeniería Metalúrgica y Química Inorgánica, Facultad de Ciencias, Universidad de Cádiz, Campus Río San Pedro, E-11510 Puerto Real (Cádiz), Spain
[b] CEA Grenoble, INAC/SP2M, 17 Rue de Martyres, 38054 Grenoble, France
[c] Departamento de Química Orgánica, Facultad de Ciencias, Universidad de Córdoba, Campus de Rabanales, Edificio C-3, Carretera Nacional IV-A, Km 396, E-14014 Córdoba, Spain

ARTICLE INFO

Article history:
Received 23 February 2010
Revised 1 March 2010
Accepted 3 March 2010
Available online 14 April 2010

Keywords:
Alumina-supported lanthana
Preparation
Calcination temperature
Nano-structure
Lanthana distribution
CO_2 adsorption
Catalytic activity
Meerwein–Ponndorf–Verley reaction

ABSTRACT

We investigate a series of three La_2O_3/Al_2O_3 samples, with a lanthana loading close to the theoretical monolayer, obtained by calcination at 773 K, 973 K, or 1173 K from a common precursor. The samples were characterized by N_2 adsorption at 77 K, X-ray diffraction (XRD), X-ray photoelectron spectroscopy (XPS), a variety of nano-analytical and nano-structural electron microscopy techniques, temperature programmed desorption (TPD-CO_2), and volumetric CO_2 adsorption techniques. By combining the information obtained from all these studies, a detailed description of their texture, nano-structure, lanthana distribution, and chemical properties could be gained. Three different forms of supported lanthana have been identified, and their relative weight evaluated quantitatively. As revealed by CO_2 adsorption, these forms show strong, weak, or not measurable surface basicity, respectively. Upon increasing the calcination temperature, a progressive inter-conversion of the co-existing lanthana forms with inherent loss of surface basicity is observed. The effect, though moderate, is particularly noticeable on the sample calcined at 1173 K. The amount of CO_2 irreversibly chemisorbed on the different samples, including the alumina support, correlates well with their catalytic activity for the Meerwein–Ponndorf–Verley reaction of cyclohexanone with 2-propanol. This behavior is discussed with reference to that expected for pure lanthana. We conclude that our supported lanthana samples represent an advantageous alternative to pure La_2O_3 as highly basic catalytic materials.

1. Introduction

In recent years, basic solid catalysts are receiving an increasing attention in the literature [1–3]. A variety of reactions have been assayed on them [4–11]. The rare earth sesquioxides, Ln_2O_3, are known to be highly basic materials, and this character smoothly decreasing throughout the lanthanoid series [1,12]. Accordingly, lanthana is the member of the Ln_2O_3 family exhibiting the highest basicity [12]. Moreover, in accordance with some experimental studies carried out on a wide series of metal oxides [13], lanthana exhibits the highest basicity amongst all the investigated materials, thus becoming an interesting candidate as active phase in processes catalyzed by basic oxides. There are, however, a number of drawbacks that strongly restrict the catalytic applications of lanthana. The most common procedures used in its preparation typically lead to low surface area samples, additional post-preparation treatments being necessary to improve their initial textural properties [14]. May be more important, in contact with atmospheric H_2O and CO_2, at room temperature, lanthana undergoes very strong textural, structural, and chemical changes [12]. Its dispersion on an appropriate oxide carrier may thus be considered as an interesting alternative to the bulk oxide reference for comparison catalytic applications.

Though a number of studies dealing with La_2O_3/SiO_2 materials are presently available [15–17], high surface area transition alumina-supported lanthana is by far the most investigated system [12]. A great majority of these studies, however, have been devoted to the investigation of La_2O_3 as textural/structural promoter of the alumina [18–21]. Typically, lanthana loadings not exceeding 10 wt.% are used in these studies. Though less detailed and numerous, some papers have also dealt with the chemical properties of Ln_2O_3/Al_2O_3 systems [22–24].

The major objective of this work is the investigation of the textural, nano-structural, surface basicity, and catalytic behavior of a series of high surface area transition alumina-supported lanthana

* Corresponding author. Fax: +34 956 016288.
E-mail address: serafin.bernal@uca.es (S. Bernal).

0021-9517/$ - see front matter © 2010 Elsevier Inc. All rights reserved.
doi:10.1016/j.jcat.2010.03.005

samples. Some recently published results for a bulk lanthanum oxide [1] will be used as a reference for comparison. The choice of the lanthana loading, 16.7 wt.%, was made in accordance with the BET surface area of the alumina support, as to reach a surface density of 5.28 La^{3+} nm^{-2}, similar to that proposed in [25] for the theoretical monolayer of lanthana supported on alumina, 5.12 La^{3+} nm^{-2}. In our work, special attention has been paid to the influence of the calcination temperature, 773 K, 973 K, or 1173 K, on the above-mentioned properties of the La_2O_3/Al_2O_3 samples. To reach this target, a wide battery of highly complementary textural, analytical, and structural techniques has been applied. Likewise, temperature programmed desorption (TPD) and volumetric adsorption of CO_2, a well-known probe molecule for basic sites [1,13,22–24], were used to characterize the surface chemistry of the investigated samples. To evaluate their catalytic behavior, the Meerwein–Ponndorf–Verley (MPV) reaction of cyclohexanone with 2-propanol, a hydrogen transfer process often used to probe basic catalysts [26–28], was assayed. The analysis of the very rich information provided with by all the above-mentioned studies has allowed us to conclude that La_2O_3/Al_2O_3 samples with a lanthana loading close to the theoretical monolayer constitute an interesting family of catalysts whose basic properties could be modulated by modifying the calcination temperature.

2. Materials and methods

The three 16.7 wt.% La_2O_3/Al_2O_3 (16.7 g of La_2O_3/100 g of supported lanthana) samples investigated in this work were prepared by incipient wetness impregnation of a commercial transition alumina (PURALOX Scfa-140) from 1 M aqueous solution of 99.9% pure $La(NO_3)_3{\cdot}6H_2O$, Alfa Aesar. The impregnated sample was dried in air, at 383 K, for 12 h, and further separated in three portions, which were calcined for 2 h, at 773 K, 973 K, and 1173 K, respectively. The resulting samples will be hereafter referred to as La_2O_3/Al_2O_3-773, La_2O_3/Al_2O_3-973, and La_2O_3/Al_2O_3-1173. The final chemical composition was confirmed by means of ICP analysis, in accordance with which the La:Al molar ratio in our lanthana-modified samples was found to be 0.06:1.00.

The volumetric N_2 adsorption at 77 K and CO_2 chemisorption at 308 K were all performed on an automatic apparatus Micromeritics, model ASAP 2020. The pre-treatments applied to the samples consisted of either an evacuation, at 473 K (2 h), under a residual pressure $<1 \times 10^{-6}$ Torr, in the case of the physisorption studies, or their heating in a flow of 5%O_2/He, at 773 K (1 h), followed by 1-h evacuation at 773 K, under a residual pressure $<1 \times 10^{-6}$ Torr, in the case of the chemisorption studies. The CO_2 adsorption experiments consisted of two successive CO_2 isotherms, P(CO_2) range: 0–300 Torr, with 1-h evacuation treatment, at 308 K, in between them.

The temperature programmed desorption studies were carried out on an experimental setup coupled to a Pfeiffer quadrupole mass spectrometer. The device was equipped with mass flow controllers and electronic control of the oven temperature. All the TPD–MS diagrams were recorded under the following conditions: amount of sample: 200 mg, He flow rate: 60 cm^3/min, heating ramp: 10 K/min. Prior to running the TPD experiments, the oxide samples were submitted to a pre-treatment routine consisting of their heating at 773 K (1 h), in a flow 5%O_2/He, followed by 1 h at 773 K, under flowing He, cooling to 298 K in a flow of He, 1-h treatment in a flow of pure CO_2, at 298 K, and finally, 2 h under flowing He, also at 298 K.

X-ray powder diffraction studies (XRD) were carried out on a Bruker instrument, model D8 Advance (radius 250 mm). The diffractograms were recorded under the following conditions: Cu Kα radiation, with graphite monochromator, scan range from 3° up to 90°, with a step size of 0.07° and a time per step of 40 s. Crystalline phases were identified by diffractogram simulation and matching with the experimental ones using Fullprof Rietveld program [29] by trial and error method of the expected phases.

The X-ray photoelectron spectra (XPS) were recorded on Kratos Axis Ultra DLD apparatus. The selected X-ray source was monochromatized Al Kα radiation (1486.6 eV). Electrostatic charging effects could be stabilized with the help of the specific device developed by Kratos. Samples were pressed into self-supported wafers, they being further calcined at 773 K (1 h) under a 5%O_2/He flow, and finally evacuated at 773 K (1 h) in the catalytic chamber attached to the spectrometer. The transfer of the samples to the analysis chamber was carried out under high vacuum conditions. A 20-eV pass energy was used to collect the spectra, and the energy resolution corresponds to a FWHM of 1.1 eV for the Au $4f_{7/2}$ peak. The collected data came from La 3d, Al 2p, O 1s, and C 1s core levels. Binding energies were referred to the C1s signal at 284.6 eV and given with an accuracy of 0.1 eV.

High Angle Annular Dark Field-Scanning-Transmission Electron Microscopy (HAADF-STEM), X-Ray Energy Dispersive Spectroscopy (X-EDS), and Electron Energy Loss Spectroscopy (EELS) studies were performed on a JEOL 2010F microscope. This instrument has a structural resolution of 0.19 nm. It is equipped with a HAADF detector, an EELS spectrometer (GIF2000 Gatan Imaging Filter), and an X-EDS Oxford INCA Energy 2000 system. Energy-Filtered Images were acquired using a JEOL3010 microscope at CEA-Grenoble. The microscope is equipped with a LaB_6 filament, an objective lens with chromatic and spherical aberration of 1.3 and 0.6 mm, respectively, and a point-to-point resolution of 0.17 nm. It is also equipped with a GIF 200 EELS filter. In order to follow the spatial distribution of both Al and La, a series of EFTEM images covering the 50–2273 V range was acquired using a 2-eV slit. A home-made script has been used to measure the image drift and to generate the Spectrum Imaging-EFTEM data cube [30]. After generating the EFTEM data cube, an EELS spectrum can be extracted from each point in the image. The distribution of elements was studied by combining HAADF images with X-EDS and EELS. The spectra were acquired using the spot and Spectrum Imaging (SI-EELS) modes. In the Spot mode, a 0.5-nm probe is fixed on a specific point of the sample, and the spectrum is acquired. Regarding the SI-EELS mode studies, a 0.5-nm probe is scanned along a specific area of the sample, and EELS spectra are recorded every 0.7–0.8 nm. In order to correlate the structural and chemical information, the HAADF signal was simultaneously obtained. In this study, the spectra with 0.3 eV energy dispersion were recorded by using an acquisition time of 3–5 s and a convergence and collection semi-angle of 8 mrad and 24 mrad, respectively. To explore the element distribution on the samples, the La/Al ratio profile has been extracted from the SI analysis. The Al and La integrated signals have been calculated from the Al–L and La–N edges using a 40-eV window for the integrated signal and a 5-eV window for the background removal. The Power Law and Hartree–Slater methods were used for the background and cross-section estimation.

The MPV catalytic assays were performed at 355 K. A two-mouthed flask was used as reactor. A flask mouth was fitted with a reflux condenser, the other one being used for sampling at regular intervals. The reaction mixture, 12 mmol of cyclohexanone, 180 mmol of 2-propanol, and 0.5 g of freshly pre-treated catalyst were continuously stirred throughout the whole experiment. Prior to the catalytic assays, all the samples were heated for 1 h, at 773 K, in a flow of synthetic air, and further cooled to 298 K under the same dynamic atmosphere. The composition of the reaction mixture was determined by taking 1 μL of the reaction mixture at different reaction times. After addition of 10 μL of toluene, the samples were analyzed by GC–MS (Gas Chromatography–Mass Spectrometry). A Varian 3900 chromatograph equipped with a

Factor Four VF-5 ms 30 m × 0.25 mm column and interfaced to a Saturn 2100 mass spectrometer was used as analytical device. High purity helium (99.999%) was used as carrier gas. The main reaction product, cyclohexanol, was identified by comparison with an authentic sample and MS analysis. Quantitative determinations were based on the measured response factors of the reactants and reaction products. Activity data were all determined at 10% conversion. Turn over frequency (TOF) values were calculated as the ratio between activity data per 1 m^2 of BET surface area of the catalysts and the surface density of CO_2 adsorption sites, as determined from volumetric adsorption.

3. Results and discussion

3.1. Textural characterization studies

The experimental N_2 physisorption isotherms recorded at 77 K for the support and the three lanthana/alumina samples are included as Supplementary material. The typology of both the whole isotherms and hysteresis loops observed in all of them is very similar, which suggests that lanthana deposition does not strongly modify the textural properties of the support. Data obtained from the analysis of these isotherms are summarized in Table 1 and Fig. 1. As deduced from the micro- and meso-pore volume data reported in Table 1, all the samples may be considered as meso-porous materials exhibiting a rather narrow mono-modal pore size distribution centered at approximately 10 nm, Fig. 1.

Lanthana deposition induces an apparent loss of BET surface area from 140 $m^2\,g^{-1}$ for Al_2O_3 to 110 $m^2\,g^{-1}$ for La_2O_3/Al_2O_3-773. However, if we estimate the surface area corresponding to the amount of alumina (0.833 g) present in 1 g of this supported oxide, 117 m^2, we may conclude that, as already outlined, the lanthana deposition actually induces a slight modification of the textural properties of the support. Table 1.

Regarding the effect of the calcination temperature, a smooth decrease in the BET surface area, from 110 $m^2\,g^{-1}$, for La_2O_3/Al_2O_3-773, to 77 $m^2\,g^{-1}$, for La_2O_3/Al_2O_3-1173, is found. In parallel, the meso-pore size distributions are slightly shifted towards higher values.

3.2. Macro-structural (XRD) characterization studies

The four investigated samples were also characterized by means of X-ray powder diffraction (XRD). The corresponding diagrams are reported in Fig. 2.

The support shows a typical diffractogram for a transition alumina, Fig. 2a. Regarding the lanthana-containing samples, the diagrams for La_2O_3/Al_2O_3-773 (Fig. 2b) and La_2O_3/Al_2O_3-973 (Fig. 2c) show almost no difference with that reported in Fig. 2a, thus suggesting that lanthana is highly dispersed in both samples. This proposal is in good agreement with an earlier study [25], in accordance with which the tridimensional growth of lanthana nano-particles supported on alumina can only be observed for surface densities above 5.12 $La^{3+}\,nm^{-2}$. In our case, the surface density of lanthanum, 5.28 $La^{3+}\,nm^{-2}$, is consistent with the above-mentioned proposal.

By contrast, the diagram for La_2O_3/Al_2O_3-1173, Fig. 2d, shows remarkable differences with respect to those reported in Fig. 2b and c. New diffraction peaks, all of them assignable to a perovskite phase, $LaAlO_3$, can be clearly observed. The occurrence of this phase is in good agreement with a number of earlier studies, in accordance with which, the calcination of La_2O_3/Al_2O_3 samples at or above 1073 K may lead to the formation of the perovskite [31,32]. It is also consistent with the occurrence of $CeAlO_3$, when

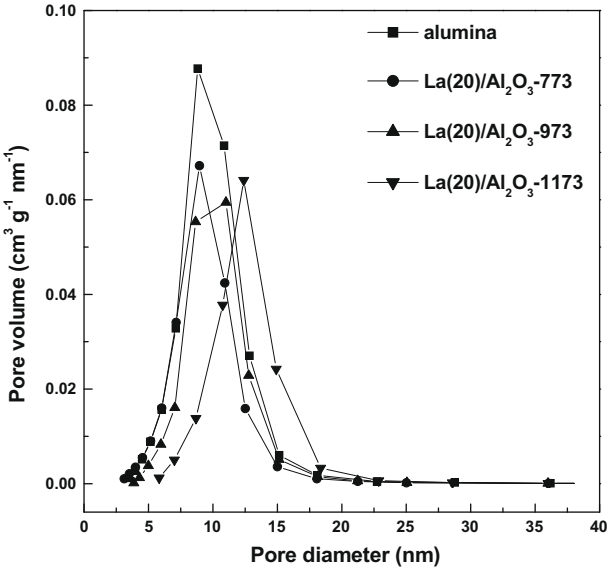

Fig. 1. Mesoporous size distribution for Al_2O_3, La(20/Al_2O_3-773), La(20/Al_2O_3-973), and La(20/Al_2O_3-1173) (as determined from the BJH analysis of the corresponding N_2 adsorption isotherms at 77 K).

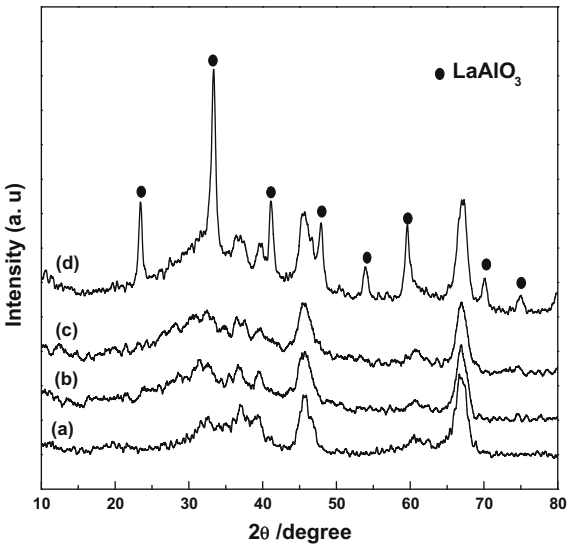

Fig. 2. X-ray diffractograms for Al_2O_3 (a), La(20/Al_2O_3-773) (b), La(20/Al_2O_3-973) (c), and La(20/Al_2O_3-1173) (d). (●) Features corresponding to the $LaAlO_3$ phase.

Table 1
Textural parameters characterizing the investigated samples as determined from N_2 adsorption at 77 K.

Sample	S_{BET} ($m^2\,g^{-1}_{sample}$)	Meso-pore volume[a] ($cm^3\,g^{-1}_{sample}$)	Mean pore diameter[a] (nm)	Micropore volume[b] ($cm^3\,g^{-1}_{sample}$)
Al_2O_3	140	0.48	9.6	0.002
La_2O_3/Al_2O_3-773	110	0.35	9.0	0.005
La_2O_3/Al_2O_3-973	96	0.35	9.9	0.005
La_2O_3/Al_2O_3-1173	77	0.33	12.4	0.005

[a] As determined by application of the BJH method to the analysis of the experimental isotherms.
[b] As determined from the analysis of the corresponding *t*-plots.

CeO_2/Al_2O_3 samples are heated under reducing conditions at temperatures in the order of 1173 K [33,34].

3.3. X-ray photoelectron spectroscopy (XPS) studies

The influence of the calcination temperature on the surface distribution of lanthana has also been investigated by means of XPS. Fig. 3 and Table 2 summarize the corresponding results. Fig. 3 shows the La $3d_{5/2}$ spectra for the three La_2O_3/Al_2O_3 samples, a clean massive La_2O_3, and a commercial perovskite, $LaAlO_3$, the latter two samples being used as reference systems. Though not shown, a parallel series of Al 2p spectra was recorded for the support, the three La_2O_3/Al_2O_3 samples, and the commercial perovskite.

In agreement with a number of earlier studies from the literature [35–37], the spectra reported in Fig. 3 consist of a main photoemission peak located at a binding energy (BE) in the range 833–835 eV and an intense satellite structure appearing at approximately 3.7 eV higher BE. This satellite has been attributed to a shake-up process, in which an electron is promoted from the filled O^{2-} 2p to empty La^{3+} 4f levels [36]. Consequently, its intensity and energy shift with respect to the main La $3d_{5/2}$ peak are affected by the local environment of the La^{3+} ions [38].

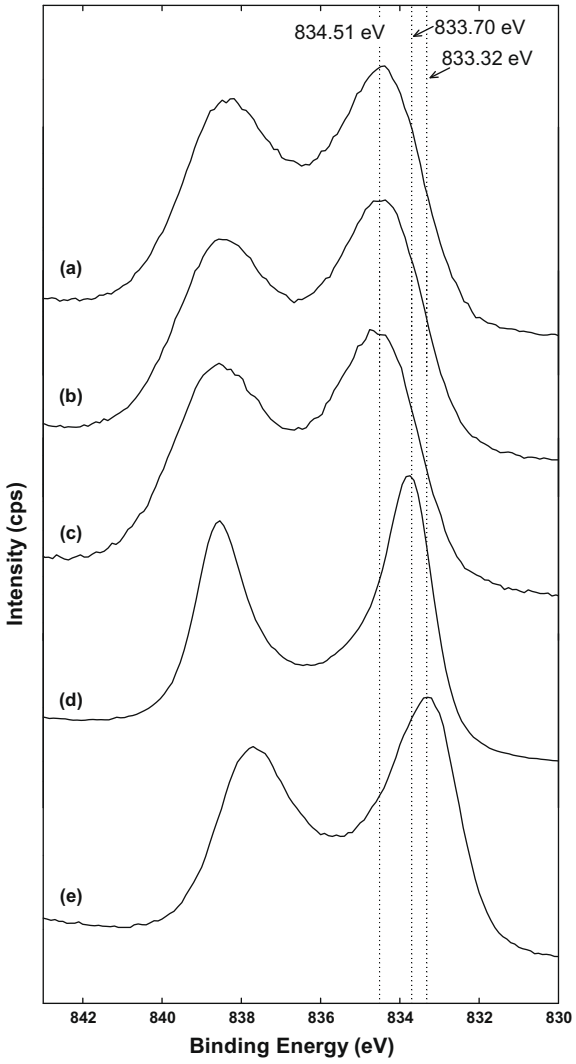

Fig. 3. La 3d5/2 X-ray photoelectron spectra for La_2O_3/Al_2O_3-773 (a); La_2O_3/Al_2O_3-973 (b), La_2O_3/Al_2O_3-1173 (c), clean La2O3 (d), and commercial $LaAlO_3$ (e).

Table 2
XPS study of the La_2O_3/Al_2O_3 samples. Pure lanthana and a commercial perovskite ($LaAlO_3$) were also investigated as reference materials.

Sample	Main La $3d_{5/2}$ (eV)	La $3d_{5/2}$ satellite (eV)	Satellite energy separation (eV)	FWHM main La$3d_{5/2}$ (eV)	Atomic ratio (La/Al)
La_2O_3/Al_2O_3-773	834.5	838.2	3.7	2.6	0.125
La_2O_3/Al_2O_3-973	834.5	838.3	3.8	2.6	0.126
La_2O_3/Al_2O_3-1173	834.6	838.4	3.8	2.7	0.087
Clean La_2O_3	833.7	838.5	4.8	1.2	–
Commercial $LaAlO_3$	833.3	837.6	4.3	1.6	1.070

As deduced from Fig. 3 and Table 2, for La_2O_3/Al_2O_3-773, the main La 3d peak and the corresponding satellite are observed at 834.5 eV and 838.2 eV, respectively, and these positions shifting very slightly with the calcination temperature up to 834.6 eV and 838.4 eV, for La_2O_3/Al_2O_3-1173. Regarding the reference samples, the main La 3d peak and its satellite are observed, respectively, at 833.7 eV and 838.5 eV, for clean La_2O_3, and at 833.3 eV and 837.6 eV, for $LaAlO_3$. We may conclude accordingly that La environment in La_2O_3/Al_2O_3 samples, though slightly modified by the calcination temperature, is significantly different from those occurring in the reference samples, i.e. clean La_2O_3 and $LaAlO_3$. This conclusion is also supported by the difference of BE between main peak and satellite in the supported lanthana samples, with values ranging from 3.7 eV to 3.8 eV, to be compared with 4.8 eV for clean La_2O_3 and 4.3 eV for $LaAlO_3$.

The different broadness of the La $3d_{5/2}$ peaks for La_2O_3/Al_2O_3 and reference samples may also be noticed. As revealed by the FWHM data reported in Table 2, the supported lanthana samples show much broader peaks, thus suggesting a larger heterogeneity in lanthanum environments.

The spectra reported in Fig. 3 for La_2O_3/Al_2O_3-1173 and $LaAlO_3$ samples are also remarkably different. Despite the occurrence of the perovskite phase, the XP-spectra for La_2O_3/Al_2O_3-1173 suggest a minor contribution of this phase to the La 3d signal.

Upon integration of the La $3d_{5/2}$ and Al 2p spectra, the corresponding La/Al atomic ratios could also be estimated. As deduced from Table 2, this ratio remains constant for La_2O_3/Al_2O_3-773 (La/Al = 0.125) and La_2O_3/Al_2O_3-973 (La/Al = 0.126), it decreasing to La/Al = 0.087 for La_2O_3/Al_2O_3-1173. The loss of surface lanthanum occurred in the latter sample is very consistent with the observation of perovskite features in the XRD diffractogram reported in Fig. 2d, as well as with the results of the electron microscopy study to be commented below.

3.4. Nano-structural (HAADF-STEM) and nano-analytical (EELS, XEDS and EFTEM) studies

Alumina-supported lanthana samples were also investigated by combining HAADF-STEM and nano-analytical techniques. In accordance with the dependence of the HAADF contrasts on the atomic number of the elements present in the sample [39], this technique is particularly suitable for the investigation into heavy elements, such as lanthanum, dispersed on light supports. Moreover, as shown in [40], high resolution HAADF-STEM may even allow the identification of atomic lanthanum dispersed on alumina.

Though HAADF imaging can provide a first view of the Al and La distributions, nano-analytical techniques are required to mapping in a finer detail these spatial distributions. Thus, by using Energy Filtering Transmission Electron Microscopy (EFTEM), element selective images were recorded on both the low- (773 K) and high- (1173 K) temperature calcined samples, Fig. 4. According to Fig. 4a and b, lanthanum is homogeneously dispersed in La_2O_3/Al_2O_3-773,

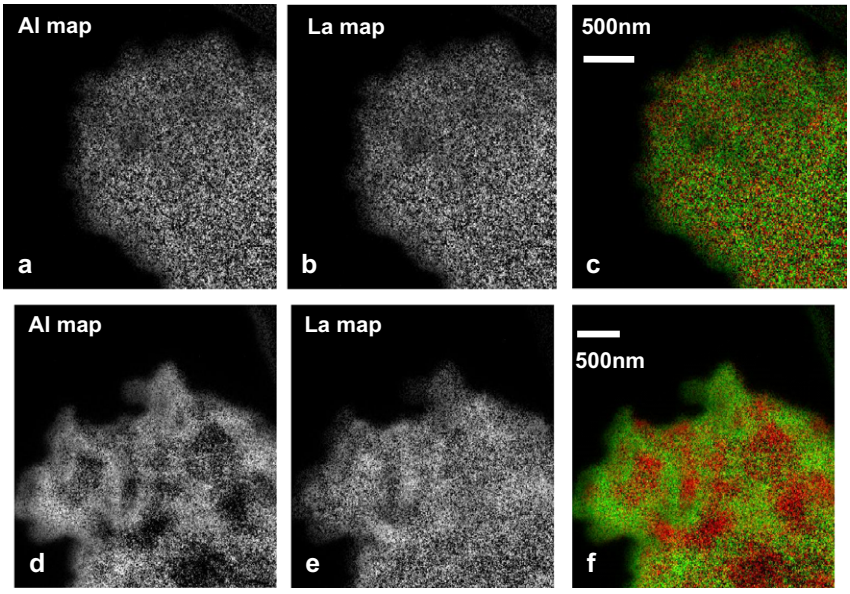

Fig. 4. Energy-Filtered TEM (EFTEM) images corresponding to La_2O_3/Al_2O_3-773 (a-Al, b-La) and La_2O_3/Al_2O_3-1173 K (d-Al, e-La). Images c and f display the color maps for Al (green) and La (red) corresponding to La_2O_3/Al_2O_3-773 and La_2O_3/Al_2O_3-1173, respectively. (For interpretation of the references to color in this figure legend, the reader is referred to the web version of this article.)

its distribution becoming much more heterogeneous on the sample calcined at 1173 K, Fig. 4d and e. This observation is fully confirmed by the color EFTEM maps (Al in green and La in red) reported, respectively, in Fig. 4c and f. As deduced from Fig. 4f, in effect, La-rich domains, a few 100 nm in size, are clearly observed in the La_2O_3/Al_2O_3-1173 sample. No similar concentration effect can be found on La_2O_3/Al_2O_3-773 (Fig. 4c).

STEM–EELS technique has also been used in this study. By operating in the so-called Spectrum Imaging (SI) mode, this technique provides very high energy and spatial resolution data on the element distribution [41]. Fig. 5 illustrates the results corresponding to La_2O_3/Al_2O_3-973. In our experiments, a 0.5-nm electron probe was scanned on the sample along the path from A to B marked in Fig. 5a, and EEL-spectra were acquired simultaneously with the HAADF signal, at 0.7-nm steps, Fig. 5b. As illustrated in the 3D plot of the whole collection of spectra, the intensity of the Al–$L_{2,3}$ (75 eV) and La–$N_{4,5}$ (100 eV) signals changes noticeably with the probe position. Fig. 5c shows the spatial variation of the La/Al ratio as determined from the quantitative analysis of this experiment. If we compare the La/Al ratio recorded in different regions of similar thickness, which may be deduced from the intensity of the HAADF signal (points 1 and 2 in Fig. 5c), we clearly observe the presence of La-enriched areas of a few nanometers in size. This suggests that, for the sample calcined at 973 K, though not detectable by the macroscopic surface analysis data provided by XPS, the lanthanum distribution starts to be modified, when compared to that shown by La_2O_3/Al_2O_3-773. The occurrence of nanometer-sized La-rich domains might thus be interpreted as an indication of the very first stages of the process of local concentration of lanthanum required for the tridimensional growth of perovskite nano-crystals.

In good agreement with the XRD and EFTEM studies reported, respectively, in Figs. 2 and 4, the HAADF images corresponding to La_2O_3/Al_2O_3-1173, Fig. 6a, indicate the presence of well-defined heavy-Z crystals due to $LaAlO_3$. Fig. 6b illustrates a gray scale image of the SI-EELS analysis performed across the region indicated on the HAADF image shown in Fig. 6a. The lines corresponding to Al–K and La–$N_{4,5}$ edges are reported. A strong variation of intensity in the La signal may be noticed, the maximum of which being reached at point 1 of the HAADF image in Fig. 6a, where a well-defined nano-particle is observed. Fig. 6c shows the EELS spectra extracted from the SI-EELS analysis corresponding to points 1 and 2. These spectra were normalized in the 160–200 eV energy loss region. As deduced from their comparison, a strong variation in the La–$N_{4,5}$ edge intensity is found, thus confirming the lanthanum enrichment associated with the contrast observed at point 1 of the HAADF image.

To summarize, the combined application of HAADF-STEM and nano-analytical techniques has proved to be a powerful tool for tracking the effect of the calcination temperature on the lanthanum distribution in the La_2O_3/Al_2O_3 samples. On La_2O_3/Al_2O_3-773, lanthana is confirmed to be well dispersed on the support. Our study has also shown that the local concentration of lanthanum starts to take place on the sample calcined at 973 K. Finally, on La_2O_3/Al_2O_3-1173, in good agreement with the XRD and XPS data, strong local concentration of lanthanum inherent to the growth of $LaAlO_3$ nano-crystallites can be clearly observed.

3.5. TPD–MS and volumetric adsorption studies on the CO_2–oxide interaction

3.5.1. Temperature programmed desorption studies

The surface basicity of the alumina and alumina-supported lanthana samples has been characterized by means of TPD–MS and volumetric adsorption techniques. In accordance with a number of earlier studies [1,12,13], carbon dioxide was used as probe molecule. Though quantitative information could also be gained from the integration of the TPD traces, the main objective of these studies was to investigate the thermal stability of pre-adsorbed CO_2. By contrast, the volumetric experiments at 308 K allowed us to obtain more precise quantitative data on both reversible and irreversible forms of adsorbed CO_2.

Fig. 7 and Table 3 summarize the results of our TPD-CO_2 study. Prior to running these experiments, the oxides were cleaned at 773 K, then they were treated with flowing CO_2 at 298 K (1 h), and finally, they were flushed with He, at 298 K (2 h). Therefore, data reported in Fig. 7 and Table 3 would mainly account for the

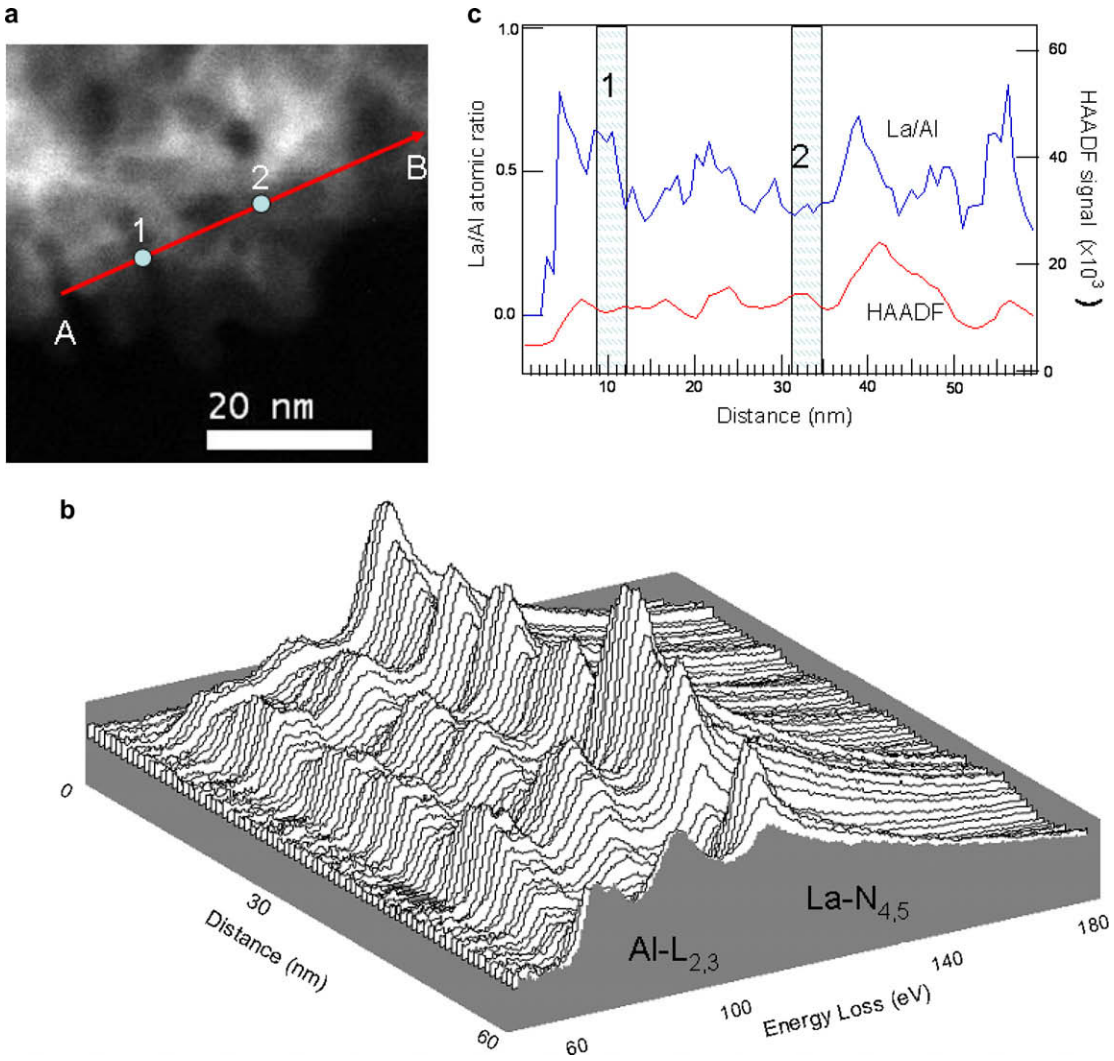

Fig. 5. Spectrum Imaging EELS (SI-EELS) analysis carried out on La_2O_3/Al_2O_3-973. (a) HAADF image where the scanned area is displayed. A 0.5-nm probe was scanned from point A to B. (b) EELS 3D plot of a collection of 80 spectra acquired along the A and B line with a step size of 0.75 nm. (c) HAADF intensity profile and La/Al ratio extracted from the EELS-SI analysis.

irreversibly adsorbed CO_2. To facilitate their comparison, the TPD signals were all referred to 1 m^2 of the BET surface area.

The dispersion of lanthana onto the alumina surface dramatically increases both the amount and thermal stability of the adsorbed CO_2. According to Table 3, the surface density of CO_2 desorbed from the support, 0.30 mol nm^{-2}, is much smaller than that determined for La_2O_3/Al_2O_3-773, 2.06 mol nm^{-2}. Likewise, the TPD-CO_2 trace for the support consists of a major desorption peak at approximately 400 K accompanied by a second much less intense feature at 835 K, the latter being probably due to a small fraction of strong basic centers occurring at the alumina surface. By contrast, the trace for La_2O_3/Al_2O_3-773, Fig. 7b, is much broader. It consists of a series of four not well-resolved features centered at approximately 400 K, 495 K, 710 K, and 920 K. It is uncertain the origin of the peak at 920 K. In accordance with Ref. [1], it could be interpreted as due to a bulk carbonate form rather than to surface species, the authors [1] only assigning to desorption phenomena the peaks observed below 773 K. Though this interpretation cannot be disregarded, the homogeneity and high dispersion of lanthana deduced from our electron microscopy study are fully consistent with the occurrence in La_2O_3/Al_2O_3-773 of a small fraction of very strong surface basic sites.

As already commented on, prior to the CO_2 adsorption, the samples were cleaned at 773 K (1 h). This temperature was selected in order not to exceed the lowest calcination temperature applied in the preparation routine. In accordance with Fig. 7, however, some desorption peaks occur at temperatures above 773 K. Therefore, the amount of CO_2 retained by the oxides after the cleaning pretreatment was also evaluated. For this purpose, TPD experiments were run on the samples submitted to the cleaning routine, without any further treatment. The corresponding diagrams are depicted in Fig. 8. As expected, the La_2O_3/Al_2O_3-773 sample, trace Fig. 8b, retains a significant amount of CO_2, the effect being progressively less important as the calcination temperature is increased. According to diagram Fig. 8a, the bare support does not retain any CO_2. The fifth column in Table 3 summarizes the quantitative data resulting from this study.

3.5.2. Volumetric adsorption studies

Two consecutive isotherms at 308 K separated by 1-h evacuation treatment at the same temperature were recorded. Fig. 9 summarizes the results of this study. Adsorption data as determined from the point-to-point difference between the first and second experimental isotherms are also plotted in Fig. 9. In this way, the total, reversible, and irreversible amounts of adsorbed CO_2, at P_{CO_2} = 300 Torr, could be determined, Table 4. The last column in this Table accounts for the irreversible adsorption data resulting from the correction of those reported in the fourth column by

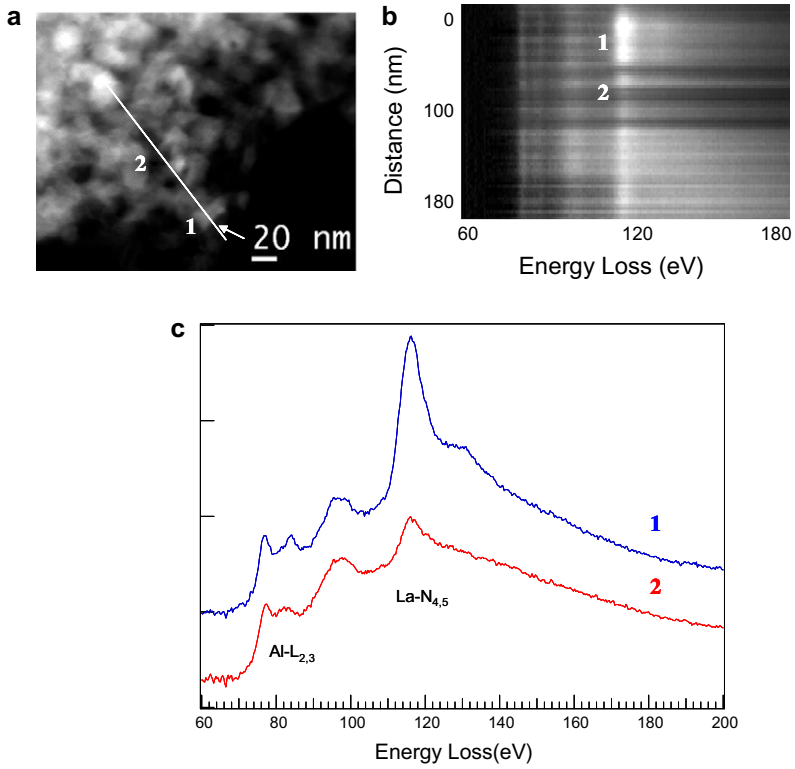

Fig. 6. Spectrum Imaging EELS (SI-EELS) analysis carried out on the La_2O_3/Al_2O_3-1173 sample. (a) HAADF image for the scanned area. (b) Gray scale image of the EEL-spectra, after background subtraction. Signals for Al-$L_{2,3}$ and La $N_{4,5}$ edges; data acquired from the area displayed in the HAADF image. (c) EEL-spectra corresponding to area 1 (crystal) and area 2 as indicated in the HAADF image.

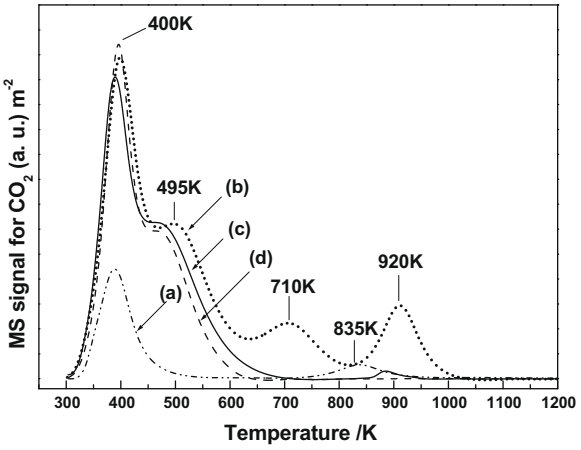

Fig. 7. TPD–MS study of CO_2 (m/e = 44) pre-adsorbed on Al_2O_3 (a), La_2O_3/Al_2O_3-773 (b), La_2O_3/Al_2O_3-973 (c), and La_2O_3/Al_2O_3-1173 (d). Prior to the CO_2 adsorption at 298 K, all the oxide samples were submitted to the standard cleaning pre-treatment at 773 K. MS signals are referred to 1 m^2 of BET surface area of the samples.

the amounts of CO_2 not eliminated during the cleaning pre-treatment, Table 3.

In good agreement with the TPD–MS study, the volumetric data fully confirm the effect of the supported lanthana on the CO_2 adsorption capability of the alumina. This effect is very strong on the irreversibly chemisorbed CO_2, 1.94 mol nm^{-2} for La_2O_3/Al_2O_3-773, to be compared with 0.22 mol nm^{-2} for Al_2O_3. Though not so strong, the influence of lanthana on the surface density of weakly adsorbed species (reversible adsorption) is also noticeable, 1.64 mol nm^{-2} for La_2O_3/Al_2O_3-773, against 0.68 mol nm^{-2} for Al_2O_3.

Table 3
Amounts of chemisorbed CO_2 as determined by integration of the corresponding TPD diagrams.

Samples	S_{BET} ($m^2\ g^{-1}$)	Total amount of desorbed CO_2[a] (μmol g^{-1})	Total amount of desorbed CO_2[a] (mol nm^{-2})	Amount of retained CO_2[b] (mol nm^{-2})
Al_2O_3	140	70	0.30	0.00
La_2O_3/Al_2O_3-773	110	376	2.06	0.21
La_2O_3/Al_2O_3-973	96	207	1.30	0.04
La_2O_3/Al_2O_3-1173	77	160	1.25	0.01

[a] As determined by integration of the TPD traces reported in Fig. 7 for the samples submitted to the cleaning routine at 773 K (1 h), and further treated with flowing CO_2 (P_{CO_2} = 1 atm), at 298 K (1 h). Prior to start the heating program, the samples were flushed with He at 298 K (2 h).

[b] As determined by integration of the TPD–MS traces reported in Fig. 8 for the samples submitted to the cleaning routine at 773 K (1 h), with no further CO_2 treatment.

Regarding the influence of the calcination temperature, data reported in Table 4 and Fig. 9 allow us to conclude that the effect is rather small on the weak adsorption sites. By contrast, the surface density of the irreversibly adsorbed forms smoothly decreases with the calcination temperature.

As already noticed, the XRD data and EFTEM maps for La_2O_3/Al_2O_3-773 clearly show that lanthana is highly and homogeneously dispersed on the alumina support. Since the surface density of lanthanum in this sample is 5.28 La^{3+} nm^{-2}, very close to the theoretical surface monolayer for lanthana supported on alumina, 5.12 La^{3+} nm^{-2} [25], we may reasonably assume that the fraction of free alumina surface in La_2O_3/Al_2O_3-773 should be very small, and therefore, that its contribution to the CO_2 adsorption could in

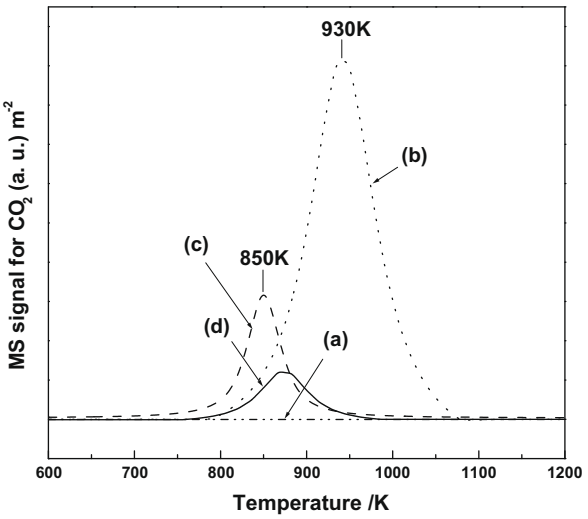

Fig. 8. TPD–MS study of the CO_2 (m/e = 44) retained by Al_2O_3 (a), La_2O_3/Al_2O_3-773 (b), La_2O_3/Al_2O_3-973 (c), and La_2O_3/Al_2O_3-1173 (d) after application of the standard cleaning procedure at 773 K, without any further CO_2 treatment. MS signals are referred to 1 m^2 of BET surface area of the samples.

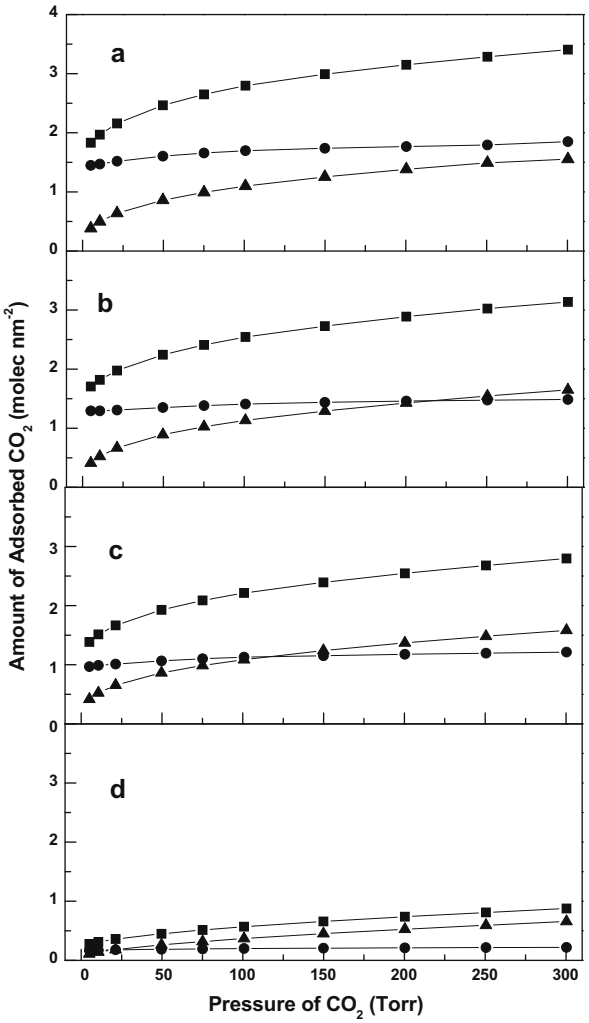

Fig. 9. First (■) and second (▲) CO_2 volumetric adsorption isotherms recorded at 308 K on La_2O_3/Al_2O_3-773 (a), La_2O_3/Al_2O_3-973 (b), La_2O_3/Al_2O_3-1173 (c), and Al_2O_3 (d). Irreversible adsorption data (●) as determined from the difference between the first and second isotherms.

Table 4
Total, reversible, and irreversible amounts of CO_2 adsorbed on the different oxide samples, as determined from volumetric studies at 308 K.

Sample[a]	Volumetric adsorption studies at 308 K (mol nm^{-2})			Corrected amount of irreversibly adsorbed CO_2[e] (mol nm^{-2})
	Total adsorbed CO_2[b]	Reversibly adsorbed CO_2[c]	Irreversibly adsorbed CO_2[d]	
Al_2O_3	0.90	0.68	0.22	0.22
La_2O_3/Al_2O_3-773	3.37	1.64	1.73	1.94
La_2O_3/Al_2O_3-973	3.25	1.73	1.52	1.56
La_2O_3/Al_2O_3-1173	3.01	1.71	1.30	1.31

[a] Prior to running the adsorption experiments, the samples were evacuated at 773 K (1 h) under high vacuum (Residual pressure <1 × 10^{-6} Torr).
[b] As determined from the first isotherm (P_{CO_2} = 300 Torr).
[c] As determined from the second isotherm (P_{CO_2} = 300 Torr).
[d] As determined from the difference between the corresponding volumetric data reported in columns 2 and 3 (P_{CO_2} = 300 Torr).
[e] As determined by the addition to the previous column the amounts of CO_2 retained by the samples after application of the cleaning routine at 773 K (last column in Table 3).

principle be neglected. If so, the upper limit for CO_2 adsorption on La_2O_3/Al_2O_3-773 could be estimated by the stoichiometric surface density of O^{2-} ions corresponding to 5.28 La^{3+} nm^{-2}; i.e. 7.92 O^{2-} nm^{-2}. However, the experimental amounts of adsorbed CO_2 reported in Table 4 are much smaller, 1.64 mol nm^{-2} for the reversible forms and 1.94 mol nm^{-2} for the irreversible ones. These values represent, respectively, the 21% and 24% of the upper limit estimated above. This is a remarkable observation indicating that, even at the lowest calcination temperature, 773 K, a 55% of the supported lanthana does not adsorb any CO_2.

To understand the quantitative data commented on above, three different types of lanthanum-containing forms ought to coexist in the La_2O_3/Al_2O_3-773 sample. The first one, that representing one fourth of the upper limit for a fully active supported phase, would be responsible for the strongest basic sites (irreversible adsorption). The second form, that accounting for the reversibly adsorbed CO_2, most likely corresponds to La_2O_3 very strongly interacting with the alumina, i.e. a sort of surface precursor of the mixed oxide phase that can only be unequivocally identified on the sample calcined at 1173 K. There is still a third fraction, that representing the 55% of the supported lantana, which does not adsorb any CO_2 probably because it is not accessible to the gas phase. We should conclude, accordingly, that the strong lanthana-alumina interaction actually implies the incorporation of lanthanum to the very first subsurface layers of the support.

With reference to La_2O_3/Al_2O_3-773, the change observed in the chemical properties of the samples calcined at 973 K and 1173 K is rather moderate. In accordance with Table 4, the surface density of the weak adsorption sites (reversible adsorption) varies very slightly. Because of the progressive loss of BET surface area, however, an effective decrease of weak adsorption sites actually occurs, very slight on La_2O_3/Al_2O_3-973 and noticeable on La_2O_3/Al_2O_3-1173. By contrast, the surface density of strong adsorption sites progressively decreases with the calcination temperature. This effect is even stronger if we take into account the parallel loss of BET surface area. Data summarizing the influence of the calcination temperature on the distribution of the lanthana forms responsible for the different chemisorption behaviors are reported in Table 5. These results were determined by applying to the surface densities of adsorbed CO_2 reported in Table 4 the correction due to the BET surface area of the corresponding samples, Table 1.

As suggested by the TPD traces for La_2O_3/Al_2O_3-773, Fig. 7b, and La_2O_3/Al_2O_3-973, Fig. 7c, the loss of surface basic sites observed upon increasing the calcination temperature may be correlated with the disappearance of the desorption peaks at 710 K and

Table 5
Distribution of lanthana adsorption sites as determined from the correction of the amounts of adsorbed CO_2 reported in Table 4 by the corresponding BET surface area of the samples.

Sample	% Irrev. ads. sites	% Rev. ads. sites	% No active ads. sites
La_2O_3/Al_2O_3-773	24	21	55
La_2O_3/Al_2O_3-973	18	20	62
La_2O_3/Al_2O_3-1173	12	15	73

920 K, those associated with the strongest basic centers. Regarding the TPD diagrams for La_2O_3/Al_2O_3-973, Fig. 7c, and La_2O_3/Al_2O_3-1173, Fig. 7d, they look like very similar, thus indicating that the nature of the active sites involved in the irreversible adsorption of CO_2 is essentially the same on both samples.

Some relevant conclusions may be drawn from the analysis of these results. With independence of the calcination temperature, the chemical properties of the supported lanthana phase are significantly different from those exhibited by the bulk oxide [1,12,14]. As shown in Table 5, the effect of increasing the calcination temperature from 773 K to 973 K would mainly consist of an increase in the inactive fraction of lanthana at the expenses of the strong adsorption sites. In parallel with this chemical modification, the electron microscopy study, Fig. 5, suggests the occurrence of some local, very slight, concentration of lanthanum. As revealed by the XPS data reported in Table 2, however, this structural change has no effect on the surface La/Al ratio, 0.125 for La_2O_3/Al_2O_3-773 and 0.126 for La_2O_3/Al_2O_3-973. We may conclude, accordingly, that the different surface basicity of the samples calcined at 773 K and 973 K is due to very subtle nano-structural changes occurring at the first surface/subsurface layers of the alumina support.

With reference to La_2O_3/Al_2O_3-773, data reported in Table 5 for La_2O_3/Al_2O_3-1173 show a noticeable loss of both reversible and irreversible adsorption sites. Likewise, the EFTEM images in Fig. 4 clearly indicate the occurrence of a remarkable concentration of lanthanum in localized nano-regions of the sample. In good agreement with this, the La/Al ratio reported in Table 2 for La_2O_3/Al_2O_3-1173, 0.087, is significantly smaller than that determined for the sample calcined at 773 K, 0.125. As confirmed by the XRD study, Fig. 2, a much stronger mobilization of the supported lanthana phase, with inherent growth of a tridimensional perovskite phase, has occurred at 1173 K. It should be stressed, however, that, even at 1173 K, the inter-conversion of supported lanthana forms is slow enough as to allow that one half of the strong basic sites in La_2O_3/Al_2O_3-773 K is still present in La_2O_3/Al_2O_3-1173 K.

3.6. Catalytic assays. Meerwein–Ponndorf–Verley reaction studies

To confirm the conclusions drawn from the characterization studies presented and discussed above, the MPV reaction of isopropanol with cyclohexanone, a process typically catalyzed by highly basic active phases [42,43], was assayed (see Scheme 1).

Table 6 summarizes the results of this study. In addition to the yield to cyclohexanol at 24 h, the table shows catalytic activity data at 10% conversion. In successive columns, activity data referred to 1 g of catalyst, 1 g of lanthanum oxide, and 1 m^2 of BET surface area are given. Likewise, by using the CO_2 adsorption data reported in Table 4, turnover frequencies could also be estimated. In this estimate, data determined by taking into account both the total surface density of adsorption sites, 5th column, and that corresponding to irreversible adsorption centers exclusively, 6th column, have been considered.

Depending on the nature CO_2 adsorption sites that are assumed to be involved in the MPV reaction, a significant difference may be noticed in the resulting turnover frequency (TOF) data. Obviously, the TOF values in the 5th column are always smaller than those reported in the 6th one, for the same catalyst. There is, however, a second difference worth of outlining. Irrespective of the catalyst, pure alumina included, TOF data in column 6 are quite close to each other, a mean value of approximately 0.17 s^{-1} being determined for all of them. This contrasts with the much wider scattering of data shown in column 5. In good agreement with earlier studies from the literature [42–44], this observation clearly indicates that the activity of the investigated catalysts for the MPV reaction can be correlated with the number of strong basic sites, i.e. those responsible for the irreversible adsorption, occurring in the assayed sample.

In accordance with the conclusions drawn from the characterization studies and catalytic assays discussed above, it is worth analyzing the interest of La_2O_3/Al_2O_3 samples as alternative highly basic catalysts to the bulk oxide. As several authors have reported [12,14], the surface density for CO_2 adsorption sites in pure lanthana is 8.0 center nm^{-2}. This value is close to 8.1 mol nm^{-2}, which was determined for a La_2O_3 sample pre-treated at 773 K by TPD-CO_2 [1]. Likewise, it is in good agreement with the stoichiometric estimate reported above for the surface density of O^{2-} ions in a monolayer of lanthana supported on alumina, 7.9 O^{2-} ion nm^{-2}. Therefore, 8.0 O^{2-} ion nm^{-2} may reasonably be used as an upper reference value for the surface density of basic sites in pure lanthana. Moreover, if it is assumed that all its surface O^{2-} ions behave as strong adsorption sites, the dispersion of lanthana on the surface of a transition alumina support would imply a decrease in the surface density of irreversible adsorption sites by, at most, a factor of 4 with respect to that expected for the bulk oxide.

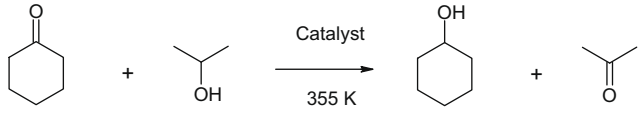

Scheme 1.

Table 6
Catalytic activity (initial rate) and yield to cyclohexanol in the MPV reaction of cyclohexanone with 2-propanol.[a]

Sample	Catalytic activity[b]			Turnover frequency (s^{-1}) × 10^{2}[b]		Yield (%)[c]
	(μmol s^{-1} g_{cat}^{-1})	(μmol s^{-1} $g_{La_2O_3}^{-1}$)	(μmol s^{-1} m^{-2})	Total CO_2 ads. sites	Irrev CO_2 ads. sites	
Al_2O_3	8	–	0.1	4	16	28
La_2O_3/Al_2O_3-773	66	395	0.3	10	19	96
La_2O_3/Al_2O_3-973	43	258	0.5	8	17	73
La_2O_3/Al_2O_3-1173	21	126	0.3	6	13	53

[a] Reaction conditions: T = 355 K; initial reaction mixture: CHON: 12 mmol; 2-propanol: 180 mmol; catalyst: 0.5 g.
[b] Data at 10% conversion.
[c] Yield to cyclohexanol at 24 h.

Despite this effect, it is important to notice that lanthana typically shows very poor textural, structural, and chemical stability [12]. As a result, the preparation of clean oxide samples requires the application thermal pre-treatments leading to low surface area materials, typically in the order or below 10 $m^2 g^{-1}$. If so, supported lanthana samples like those investigated here could compensate their lower density of strong adsorption sites with their much higher BET surface area. Thus, if a pure lanthana sample, with a surface density of irreversible adsorption sites of 8.0 center nm^{-2} and 10 $m^2 g^{-1}$, is compared with our La_2O_3/Al_2O_3-773, we may conclude that, in the latter, the amount of strong adsorption sites per gram of sample is 2.8 times larger. Even for La_2O_3/Al_2O_3-1173, this amount is still 1.3 times larger than that for the bulk oxide used as reference. Obviously, the difference in favor of the supported samples would be much larger if the number of strong adsorption sites is referred to 1 g of La_2O_3. We may conclude, accordingly, that the dispersion on high surface area alumina supports of lanthana loadings close to the theoretical monolayer provides with us an interesting alternative family of basic catalysts. Despite the significant loss of surface density of basic sites inherent to the dispersion process, the very much improved textural, structural, and chemical stability of the resulting catalysts allows them to compete with bulk oxide samples advantageously. Moreover, as shown in this work, the surface basicity of the supported lanthana catalysts may be modulated by varying the calcination temperature in a wide range of values, from 773 K to 1173 K, with no dramatic loss of active sites.

4. Conclusions

To summarize, the combined application of a wide battery of textural (N_2 adsorption at 77 K), chemical (volumetric adsorption and TPD–MS of CO_2), surface analysis (XPS), nano-analytical (X-EDS, EELS, SI-EELS), and nano-structural (HAADF-STEM) techniques has allowed us to gain a detailed picture of the chemical and nano-structural properties of a series of La_2O_3/Al_2O_3 samples with a lanthana loading close to the theoretical monolayer. Special attention has been paid to the study of the influence of the calcination temperature on the above-mentioned properties. Even at the lowest calcination temperature, 773 K, the chemical properties of the supported lanthana phase are significantly modified by its interaction with the alumina. As much as 55% of the supported lanthana shows no activity against CO_2 adsorption, a progressive, though moderate, loss of active sites being observed as the calcination temperature is increased at 973 K and 1173 K Despite this, in principle, not desirable effect, the reported results clearly prove that, in addition to show a higher number of strong surface basic sites per unit of mass of sample, the supported lanthana samples exhibit a much better textural, chemical, and structural stability than pure lanthana. Moreover, the distribution of surface basic sites in the supported samples may be modulated by the calcination temperature, thus allowing us to design catalytic materials in accordance with the specific requirements of the investigated reaction. The advantages of dispersing lanthana on a high surface area transition alumina are fully confirmed by the assay of the MPV reaction of isopropanol with cyclohexanone, a process typically used in the evaluation of highly basic catalytic materials.

Acknowledgments

This work has been supported by the Ministry of Science and Innovation of Spain/FEDER Program of the EU (Project: MAT 2008/00889-NAN) and the *Junta de Andalucía* (Project: FQM-262; Groups FQM-110 and FQM-334). L.F and Z.B acknowledge their MAEC-AECI Grants. ST acknowledges the MEC "Ramón y Cajal" and "José Castillejo" Programs. The STEM-HAADF, EELS, XRD, and XPS studies were carried out at UCA Facilities. EFTEM experiments were performed at CEA-Grenoble in collaboration with Dr. Pascale Bayle-Guillemaud INAC/SP2M/LEMM.

Appendix A. Supplementary material

Supplementary data associated with this article can be found, in the online version, at doi:10.1016/j.jcat.2010.03.005.

References

[1] S. Sato, R. Takahashi, M. Kobune, H. Gotoh, Appl. Catal. A: Gen. 356 (2009) 57.
[2] S. Valange, A. Beauchaud, J. Barrault, Z. Gabelica, M. Daturi, F. Can, J. Catal. 251 (2007) 113.
[3] S. Bancquart, C. Vanhove, Y. Pouilloux, J. Barrault, Appl. Catal. A: Gen. 218 (2001) 1.
[4] X. Zhang, A.B. Walters, M.A. Vannice, J. Catal. 155 (1995) 290.
[5] K. Tanabe, W.F. Hölderich, Appl. Catal. A: Gen. 181 (1999) 399.
[6] S. Sato, R. Takahashi, T. Sodesawa, A. Igarashi, H. Inoue, Appl. Catal. A 328 (2007) 109.
[7] C. Ngamcharussrivichai, P. Totarat, K. Bunyakiat, Appl. Catal. A: Gen. 341 (2008) 77.
[8] X. Liu, X. Piao, Y. Wang, S. Zhu, H. He, Fuel 87 (2008) 1076.
[9] A. Kawashima, K. Matsubara, K. Honda, Bioresour. Technol. 99 (2008) 3439.
[10] H. Ma, S. Li, B. Wang, R. Wang, S. Tian, J. Am. Oil Chem. Soc. 85 (2008) 263.
[11] A. D'Cruz, M.G. Kulkarni, L.C. Meher, A.K. Dalai, J. Am. Oil Chem. Soc. 84 (2007) 937.
[12] S. Bernal, G. Blanco, J.M. Gatica, J.A. Pérez Omil, J.M. Pintado, H. Vidal, Chemical reactivity of binary rare earth oxides, in: G. Adachi et al. (Eds.), Binary Rare Earth Oxides, Kluwer Academic Publishers, 2004, pp. 9–55 (Chapter 2).
[13] A. Auroux, A. Gervasini, J. Phys. Chem. 94 (1990) 6371.
[14] M.P. Rosynek, D.T. Magnuson, J. Catal. 46 (1977) 402.
[15] H. Vidal, S. Bernal, R.T. Baker, D. Finol, J.A. Pérez Omil, J.M. Pintado, J.M. Rodríguez-Izquierdo, J. Catal. 183 (1999) 53.
[16] G.A.H. Mekhemer, Phys. Chem. Chem. Phys. 4 (2002) 5400.
[17] G. Blanco, J.J. Calvino, M.A. Cauqui, G.A. Cifredo, J.A. Pérez Omil, J.M. Rodriguez-Izquierdo, H. Vidal, J. Alloys Compd. 207–208 (1994) 201.
[18] H. Schaper, D.J. Amesz, E.B.M. Doesburg, L.L. Van Reijen, Appl. Catal. 9 (1984) 129.
[19] P. Burtin, J.P. Brunelle, M. Pijolat, M. Soustelle, Appl. Catal. 34 (1987) 239.
[20] F. Oudet, P. Courtine, A. Vejeux, J. Catal. 114 (1988) 112.
[21] H. Arai, M. Machida, Appl. Catal. A: Gen. 138 (1996) 161.
[22] L.P. Haack, J.E. de Vries, K. Otto, M.S. Chattha, Appl. Catal. A: Gen. 82 (1992) 199.
[23] T. Yamamoto, T. Tanaka, T. Matsuyama, T. Funabiki, S. Yoshida, J. Phys. Chem. B 105 (2001) 1908.
[24] H. Zou, X. Ge, J. Shen, Thermochim. Acta 397 (2003) 81.
[25] M. Bettman, R.E. Chase, K. Otto, W.H. Weber, J. Catal. 117 (1989) 447.
[26] C. Jiménez-Sanchidrián, J.M. Hidalgo, J.R. Ruiz, Appl. Catal. A: Gen. 303 (2006) 23.
[27] J.R. Ruiz, C. Jiménez-Sanchidrián, Curr. Org. Chem. 11 (2007) 1113.
[28] M. Glinski, Appl. Catal. A: Gen. 349 (2008) 133.
[29] J. Rodriguez-Carvajal, Physica B 192 (1993) 55.
[30] P. Bayle-Guillemaud, G. Radtke, M. Sennour, J. Microsc.-Oxford 210 (2003) 66.
[31] T. Yamamoto, T. Tanaka, T. Matsuyama, T. Funabiki, S. Yoshida, J. Synchrotron Radiat. 8 (2001) 634.
[32] B. Beguin, E. Garbovski, M. Primet, Appl. Catal. A 75 (1991) 119.
[33] S. Bernal, G. Blanco, G.A. Cifredo, J.J. Delgado, D. Finol, J.M. Gatica, J.M. Rodriguez-Izquierdo, H. Vidal, Chem. Mater. 14 (2002) 844.
[34] T. Miki, T. Ogama, M. Haneda, N. Kakuta, A. Ueno, S. Tateishi, S. Matsura, M. Sato, J. Phys. Chem. 94 (1990) 6464.
[35] A. Galtayries, G. Blanco, G.A. Cifredo, D. Finol, J.M. Gatica, J.M. Pintado, H. Vidal, R. Sporken, S. Bernal, Surf. Interface Anal. 27 (1999) 941.
[36] P. Burroughs, A. Hamnett, A.F. Orchad, G. Thornton, J. Chem. Soc., Dalton Trans. 17 (1976) 1686.
[37] Y. Uwamino, T. Ishizuka, H. Yamatera, J. Electron Spectrosc. Relat. Phenom. 34 (1984) 67.
[38] H.H. Berthou, C.K. Jørgensen, C. Bonelle, Chem. Phys. Lett. 38 (1976) 199.
[39] S.J. Pennycook, D.E. Jesson, Ultramicroscopy 37 (1991) 14.
[40] S. Wang, A.Y. Borisevich, S.N. Rashkeev, M.V. Glazoff, K. Sohlberg, S.J. Pennycook, S.T. Pantelides, Nat. Mater. 3 (2004) 143.
[41] C. Jeanguillaume, C. Colliex, Ultramicroscopy 28 (1989) 252.
[42] V.A. Ivanov, J. Bachelier, F. Audrey, L.C. Lavalley, J. Mol. Catal. 91 (1994) 45.
[43] M.A. Aramendia, V. Borau, C. Jiménez, J.M. Marinas, J.R. Ruiz, F.J. Urbano, Appl. Catal. A: Gen. 249 (2003) 1.
[44] J. López, J. Sanchez Valente, J.M. Clancens, F. Figueras, J. Catal. 208 (2002) 30.